Aligned Polythiophene and its Blend Film by Direct-Writing for Anisotropic Charge Transport

Guanghao Lu, Jiayue Chen, Wentao Xu, Sijun Li and Xiaoniu Yang**

A combination of patterning and film alignment techniques helps to build multi-order polymer architecture for application in flexible electronics. A direct-writing method is employed using microcapillary arrays to prepare semiconducting polymer films with both optical and electrical anisotropy. Not only aligned poly(3-butylthiophene) (P3BT) nanowires in neat P3BT films, but also aligned P3BT nanowires within a polystyrene (PS) matrix are obtained, which yields an aligned semiconductor/insulator polymer blend with anisotropic charge transport. The field-effect transistor (FET) mobilities/threshold voltages from both vertical and parallel to alignment directions as well as their dependence on blending ratio are studied. The increased mobility of P3BT/PS blends, as compared with neat P3BT, is observed in both vertical and parallel directions. Using this alignment method, FET mobility and threshold voltage of the semiconductor/insulator polymer blends are comprehensively tuned, from which a digital inverter with gain up to 80 is realized. Therefore, this work not only helps understanding the charge transport mechanism in semiconducting/insulating polymer blends, but also provides an effective approach towards high-performance field-effect transistors with tunable mobility and threshold voltage.

1. Introduction

Conjugated-polymer thin films have attracted wide interest due to their low-cost and solution processability. Patterning techniques for these films, such as lithography and printing, play an important role in the fabrication of polymer-based flexible electronics.[1–4] A combination of patterning and film alignment techniques helps to build multi-order architectures. For instance, the alignment of conjugated polymers has attracted great attention, and epitaxy,[5–7] micro-mold,[8,9] dip-coating/zone casting,[3,10,11] rubbing,[12] strain,[13] confinement-induced crystallization,[14,15] and solvent vapor treatment/controlled solvent evaporation[16,17] have been employed to tune the alignment of polythiophene and thus the anisotropy properties.[18,19] However, so far the combination of patterning techniques and crystalline alignment still does not meet the requirement of practical applications. Direct-writing[20,21] from solution is a newly developed technique, which has already demonstrated a high output efficiency and fidelity. In a typical direct-writing process, polymer solution is extruded from a nozzle and deposited onto a substrate. Here, we report the hydrodynamic-assisted nematic alignment of poly(3-butylthiophene) (P3BT)[22–24] nanowires within a capillary tube, from which we not only prepare aligned P3BT nanowires in a neat P3BT film, but also aligned P3BT nanowires in a polystyrene (PS) matrix, forming an aligned semiconductor/insulator polymer blend. Actually, in recent years semiconductor/insulator polymer blends[25–38] are attracting more and more interests due to the high field-effect-transistor (FET) performance, mechanical robustness and low cost. FET performance based on these composites with less than 10% semiconductor is comparable to or higher than that of neat semiconductor. To the best of our knowledge, the FET performance of aligned semiconductor/insulator polymer blends has not yet been investigated. On the other hand, several mechanisms were proposed to interpret the high FET performance of semiconductor/insulator polymer blends, which include 1) enrichment of semiconductor on film top[39] or bottom surface;[27,40] 2) enhanced crystallinity;[27] 3) zone-refinement;[41] 4) enhanced semiconductor/insulator interface.[42,43] However, the role of insulating-matrix on the transistor properties of semiconductor is still unclear and/or in debate. In these composites, semiconductors are crystalline and these nanowire-like domains are connected with each other to form a charge transport network.[44] Here we studied inter-domain and intra-domain charge transport by investigating anisotropic field-effect transistor properties of aligned P3BT nanowires within PS matrix, which helps understand the charge transport in semiconductor/insulating-polymer blends. The increased mobility of P3BT/PS blends, as compared with neat P3BT, is observed in both vertical and parallel directions.

Dr. G. Lu, J. Chen, W. Xu, Dr. S. Li,[+] Prof. X. Yang
State Key Laboratory of Polymer Physics and Chemistry
Changchun Institute of Applied Chemistry
Chinese Academy of Sciences
Renmin Str. 5625, Changchun 130022, P. R. China
E-mail: guanghao.lu@hotmail.com; xnyang@ciac.jl.cn
Dr. G. Lu
Department of Polymer Science and Engineering
University of Massachusetts,
Amherst, 120 Governors Drive, Massachusetts 01003, USA

[+]Present address: Electron Microscopy for Materials Research (EMAT), University of Antwerp, Groenenborgerlaan 171, 2020 Antwerp, Belgium.

DOI: 10.1002/adfm.201400699

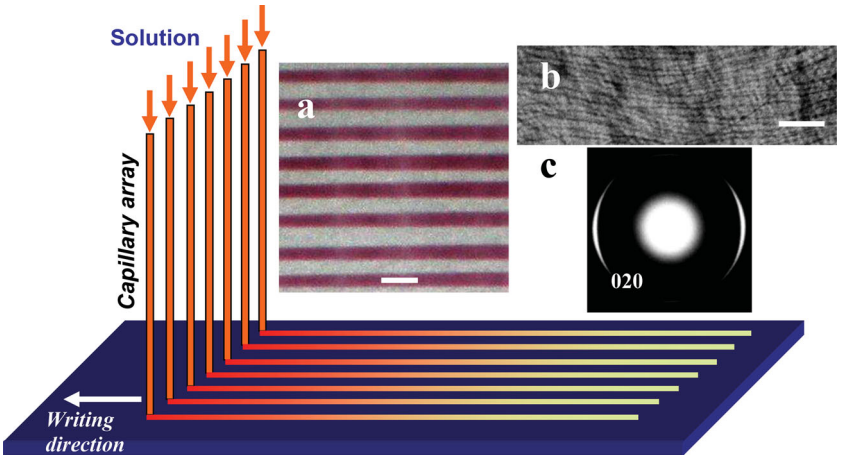

Figure 1. Scheme: Direct-writing by capillary array. Micrographs: optical microscopy image (scale bar 1000 μm) (a) and TEM image (scale bar 200 nm) (b) of polymer stripes prepared by direct writing. (c) A typical selected area electron diffraction.

2. Results and Discussion

In this section, we use P3BT to demonstrate how direct writing induces nematic alignment, and the material was then intensively investigated in terms of both optical anisotropy and electrical anisotropy. Subsequently, direct writing was employed to obtain aligned P3BT/PS blends, of which the field-effect mobility and threshold voltage were found to be dependent on the blending ratio and alignment directions. Finally, we use a digital inverter prototype to demonstrate the application of our aligned materials with comprehensively tunable mobility and threshold voltage.

2.1. Aligned P3BT and Optical Anisotropy

P3BT was dissolved in *o*-dichlorobenzene (ODCB) at 80 °C. After cooling to room temperature, P3BT chain gradually crystallizes in solution. In **Figure 1**, we schematically show the direct-writing process from P3BT solution, using a capillary array. The optical microscopy (OM) (Figure 1a) image shows a polymer stripe array prepared via direct writing. The transmission electron microscopy (TEM) image (Figure 1b) indicates that the stripe is composed of P3BT nanowires (nanowire width ~ 20 nm),[22,45] and the nematic alignment of P3BT nanowires is parallel to the writing direction.

In order to quantitatively determine the angle distribution of P3BT nanowires in the polymer stripes, we recorded cross-polarizer optical microscopy (CPOM) images and measured their brightness (upon integrating the gray scale of each pixel of the image (330 pixels × 2340 pixels) in the stripe area (**Figure 2**a) as a function of direction of cross-polarizers (Figure 2b). Under our experimental conditions, the image brightness is approximately proportional to the light intensity received by the CCD camera. According to the principle of birefringence, the intensity of light (I) propagated through a pair of cross-polarizers (polarizer and analyzer) inserted by an optical uniaxial crystal can be written as $I \propto \sin^2 2\theta(1+\cos\Delta\phi)$, where θ is the angle between polarizer and electric field direction of *e*-light in crystal, and $\Delta\phi$ is phase difference. So the minimum and maximum of intensity can be calculated as $\theta = 180°n/2$ and $\theta = (360°n+180°)/4$, respectively.[14] Correspondingly, the light has a minimum intensity I at $\theta = 0°$, 90°, 180°, 270°, and maximum intensity at θ = 45°, 135°, 225°, 315°. Figure 2b clearly shows that the maximum and minimum brightnesses of the image obey this rule.[46]

However, the polymer stripe is not a single crystal; it is actually composed of aligned P3BT nanowires, of which the angles might depart from the writing direction. We used numerical simulations to calculate the angle distribution of P3BT nanowires and so to assess the nematic alignment. The angle deviation of the crystalline domain is within the range [−90°, 90°], and the angle distribution of these crystalline domains can be described by $(1/\sigma)\exp[-(\alpha_i)^2/(2\sigma^2)]$, where σ the is standard deviation. So the intensity of CPOM can be re-written as the convolution of angle distribution of crystalline domains with the composed light density passed through cross-polarizers:[14]

$$I \propto \sum_{i=1}^{n} g(\theta+\alpha_i)(1/\sigma)\exp[-\alpha_i^2/(2\sigma^2)]\sin^2 2(\theta+\alpha_i) \quad (1)$$

where $g(\theta+\alpha_i)$ is a polarized absorption factor (obtained from single-polarizer optical microscopy). A least squares criterion was used to fit σ. From the fitting result we obtain the average angle deviation $<|\alpha|> = 12.8°$ (see Supporting Information), and the angle distribution is given in Figure 2c.

Afterwards we calculated the 2-dimensional orientation parameter $f = 2 < \cos^2\alpha > -1$ (see Supporting Information) proposed by Stein[47,48] as figure of merit of the polymer stripe.

According to Equation (1), ideally we have $f = 0$ for random orientation and $f = 1$ for perfect orientation. In this work, f = 0.85 was obtained from the simulated angle distribution, as shown in Figure 2c, which is a relatively high value and implies that the polymer film generated from direct writing is highly aligned. Out-of-plane orientation of P3BT domains was evaluated by grazing incidence angle X-ray diffraction (GIXRD) measurements, which show that the pi–pi packing direction is mostly within the substrate/film plane (Figure S1).

In order to illuminate the mechanism for these highly aligned P3BT crystals within the stripes, one question certainly should be answered, i.e., what's the driving force for the alignment? Let's look at the preparation conditions of P3BT in the solvent ODCB. The solution was first prepared by heating to 70–80 °C to get a completely dissolved P3BT. After cooling to room temperature and then keeping for 72 h, P3BT gradually self-assembles into nanowires in the poor solvent ODCB.[42,49,50] Correspondingly, the color of the solution gradually changed from orange to purple. Here, in order to confirm that the nanowires were formed in solution[42,51] rather than formed during solvent evaporation, and to assess the relaxation/Brownian motion of the P3BT nanowires during solvent evaporation, we measured the optical anisotropy of P3BT solution in-situ in the capillary

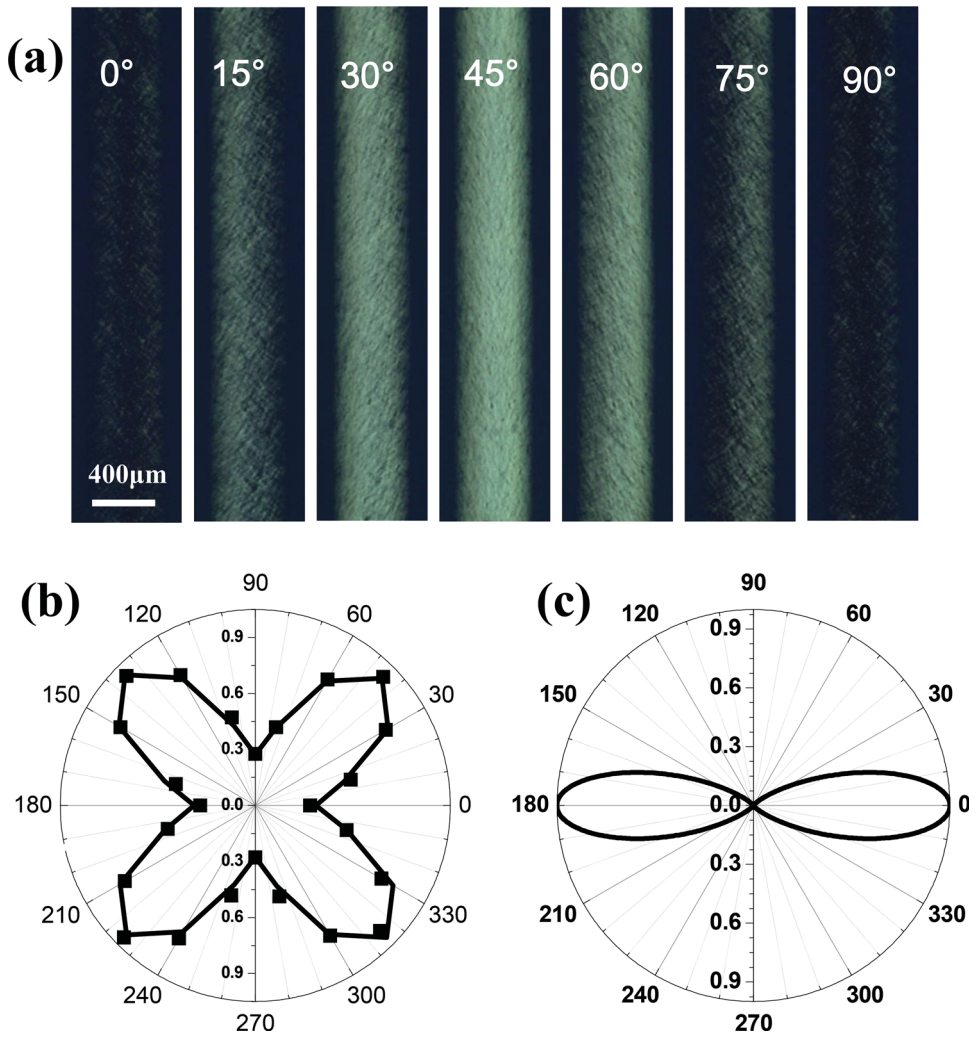

Figure 2. Optical anisotropy of P3BT stripes. a) In-situ CPOM study of a stripe. The angles between polarizer and direct-write direction are shown in each corresponding micrograph. b) Experimental CPOM intensity (solid squares) and fitted CPOM intensity (curve). c) Simulated angle distribution of crystalline domains departed from direct-writing direction.

(**Figure 3**). The strong birefringence implies the crystalline nature of the P3BT in solution. Correspondingly, the light intensity reaches its minimum at $\theta = 0°$, 90°, 180°, 270° and maximum at $\theta = 45°$, 135°, 225°, 315°, which shows that the P3BT nanowires have already been aligned along the capillary direction. Accordingly, the average angle deviation is $<|\alpha|> = 14.0°$, and the 2D orientation parameter is $f = 0.83$, which is consistent with the alignment in dried P3BT stripes (Figure 2). Moreover, the angle distribution of P3BT nanowires in the capillary is similar to that within the dried stripes. This result also confirms that, during solvent evaporation, both conformation relaxation and Brownian motion of P3BT nanowires are not pronounced, at least on the scale of either micrometers in terms of space and minutes in terms of time. The inhibition of conformation relaxation and Brownian motion during solvent evaporation preserves the alignment of P3BT nanowires.

According to Newton's law of viscosity and Poiseuille's equation, the flow velocity of fluid in capillary can be described by $v \propto R^2\text{-}r^2$, where R is the radius of capillary and r is the distance from the center of the capillary (see Supporting Information and Figure S2,3). So the alignment of P3BT nanowires within the solution should be due to the shear force derived from the flow gradient. The manipulation of inorganic nanowires[52,53] via liquid flow has been studied, where the hydrodynamic force plays a crucial role.

According to Onsager's theory, the critical volume fraction of rigid rods in solution for nematic order is $\phi = 3.3d/L$, where d is the diameter and L is the length of the rod.[54,55] Because the concentration of P3BT solution used for this work is ca. 1% in volume, the average aspect ratio (L/d) of P3BT nanowires in solution should be larger than 300 for effective nematic alignment, which is consistent with morphological observations using TEM and AFM.[42,43] Upon using capillary-assisted direct writing, we even observed nematic alignment of P3BT with volume fractions lower than 0.1%. This low value is related to the confined microscale liquid flow in the capillary and the super long length of the P3BT nanowires.

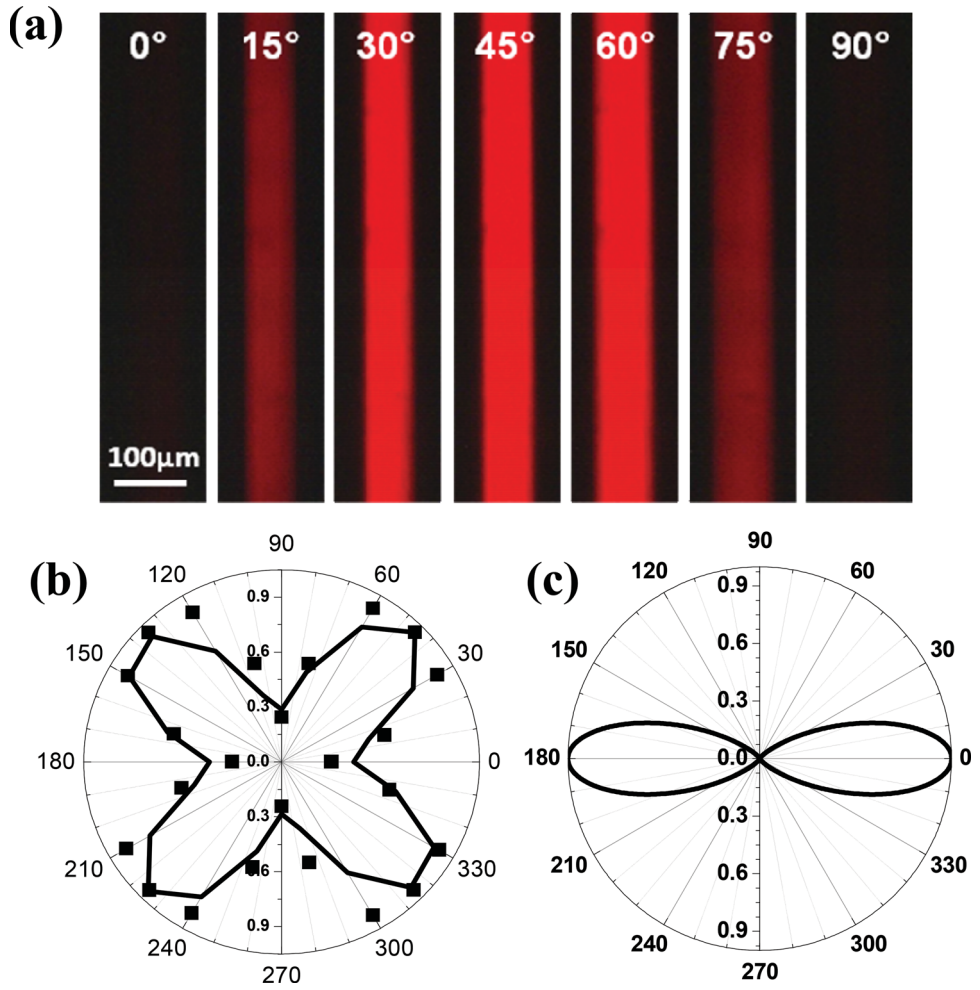

Figure 3. Optical anisotropy of P3BT nanowires in-situ in the capillary. a) In-situ CPOM study of P3BT nanowires in solution in capillary. The angles between polarizer and capillary direction are shown in each corresponding micrograph. b) Experimentally determined CPOM intensity (solid squares) and fitted CPOM intensity (curve). c) Simulated angle distribution of crystalline domains departed from capillary direction.

2.2. Anisotropic Charge Transport in Aligned P3BT

Above, we quantitatively investigated the optical anisotropy of P3BT nanowires in solution and film by optical birefringence (Figures 2,3). Direct writing of semiconducting polymers can potentially be used in the fabrication of microelectronic devices, since this technique has exhibited both high throughput and fidelity. The investigation of the film with aligned polythiophene nanowires definitely helps to clarify a still-unclear scientific issue, i.e., the anisotropic charge carrier transport. Subsequently, we used this aligned film as the semiconducting layer to fabricate a field-effect transistor (FET). **Figure 4** shows the output and transfer characteristics of FET devices with charge transport directions both along and vertical to the writing direction of neat P3BT. The field-effect mobility along the alignment direction is apparently higher than that in the vertical direction. The typical mobilities along and vertical to the direct writing direction are 0.01 cm^2 V^{-1} S^{-1} and 0.004 $cm^2V^{-1}S^{-1}$, respectively, as calculated from the saturation region.

2.3. Aligned P3BT/PS Blends and Their Anisotropic Charge Transport

We have previously shown that P3BT could be homogenously distributed with polystyrene (PS) matrix.[42,43,56] In this work, aligned P3BT nanowires were also achieved within PS matrix via direct writing. We used this aligned P3BT within a PS matrix as a semiconducting layer to fabricate an FET. **Figure 5** shows the output and transfer characteristics of FET devices with the charge transport directions (from source to drain electrode) parallel and vertical to writing direction. The output and transfer curves imply good OFET performance of P3BT/PS (4 wt% P3BT) in both directions (in terms of parallel and vertical charge transport). For the transistor working in a saturated regime, the saturated mobility obeys $\mu_{sat} \propto d(-I_{ds})^{0.5}/d(-V_g)$. As shown in **Figure 6**a, for both parallel and vertical charge transport, $d(-I_{ds})^{0.5}/d(-V_g)$ rapidly increases with the negative shift of V_g. It is shown that at low $|V_g|$ the field-effect mobility parallel to the alignment direction (μ_p) is apparently higher than that of the vertical direction (μ_v), although

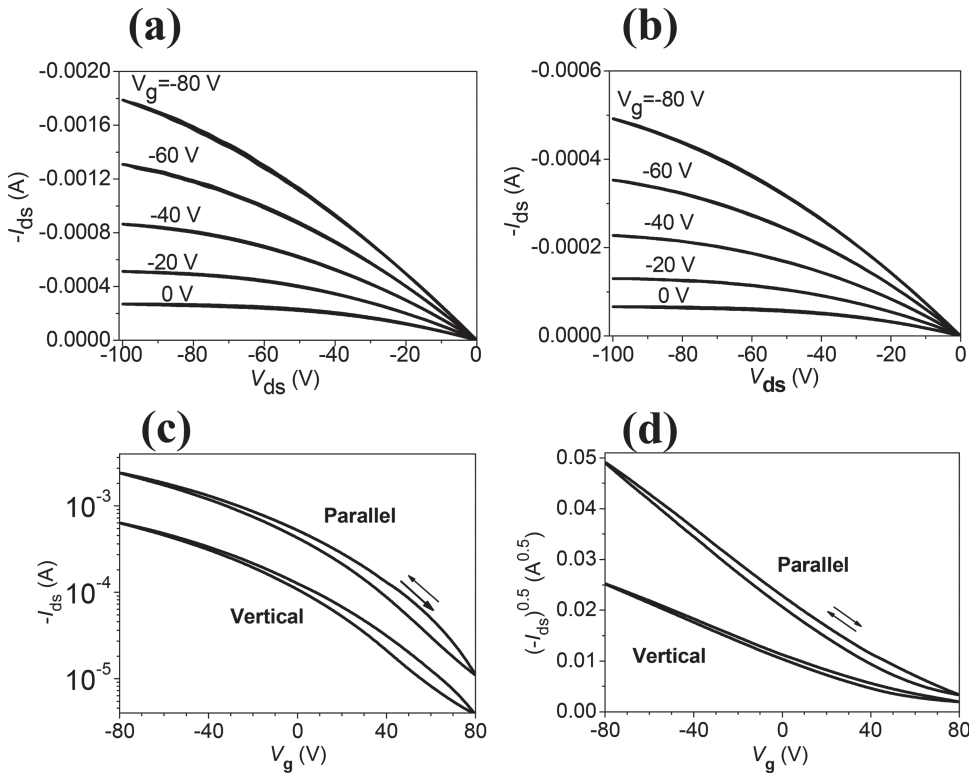

Figure 4. FET characteristics of aligned P3BT in neat P3BT film. a,b) Output characteristics of FET devices with source–drain currents parallel (a) and vertical to the alignment direction (b). c,d) Corresponding transfer characteristics (c) (V_{ds} = –100 V) and dependence of $(-I_{ds})^{0.5}$ on V_g.

both of them increase to a maximum of around 0.03–0.05 $cm^2 V^{-1}s^{-1}$ when V_g reaches –50 V or more (negative). The dependence of charge transport anisotropy (μ_p/μ_v) (Figure 6b) on V_g implies that for V_g between 0 V and –10 V, the μ_p is about one order higher than μ_v, while μ_p/μ_v rapidly decreases towards 1–2 when more holes are accumulated in the channel. Note the mobility in Figure 6b is from a saturated regime, while the transport anisotropy (μ_p/μ_v) from a linear regime has a similar dependence on gate bias.

In order to understand the dependence of charge transport anisotropy on gate bias, we performed CPOM and TEM measurements on P3BT/PS (Figure 6c). The morphology confirmed the orientation of P3BT nanowires within PS matrix. However, the overlap between P3BT nanowires forms the bridge where inter-domain charge hopping takes place. From this point of view, the inter-domain charge hopping plays a more important role for μ_v, as compared to μ_p.

P3BT is a semicrystalline conjugated polymer, and the crystalline chain is in the central part of the nanowire, while amorphous chains locate at the surface of the nanowire or between crystalline domains.[57–59] Therefore, the inter-domain charge transport needs to overcome these amorphous chains. However, the HOMO level of amorphous poly(3-alkythiophene) P3AT is about 300 meV lower than that of crystalline P3AT.[24,60,61] 300 meV is enough to significantly prevent charge hopping, because the width of the density of states (DOS) is typically ~100 meV for highly ordered polythiophene films.[62] This energetic barrier between crystalline P3BT and amorphous P3BT is responsible for the high μ_p/μ_v as observed at low $|V_g|$.

However, the accumulation of hole charges in P3BT crystalline domains lifts up the energy level of localized states as a result of Coulombic interactions between holes. The Coulombic repulsion energy E_{coul} between two individual holes is $E_{coul} = e^2/(4\pi\varepsilon_0\varepsilon r)$, where r is the distance between the holes. So $E_{coul} \approx 100$ meV when $r = 5$ nm. However, increasing $|V_g|$ accumulates more holes. Considering that the cross-section of the P3BT domain is around 15–20 nm × 5 nm,[18] and from $E_{coul} = \sum ie^2/(4\pi\varepsilon_0\varepsilon r_i)$ in the case of one hole surrounded by i holes, we get $E_{coul} > 300$ meV when the average distance between holes is $\langle r_i \rangle = 5$ nm in one P3BT crystalline domain. Because 300 meV is compared to the HOMO offset between amorphous P3BT and crystalline P3BT[24,60,61] as we mentioned above, once the gate-induced charge density is larger than $10^{19}/cm^3$, more charge will possibly occupy the amorphous P3BT chain. Taking the film thickness (~50 nm) into account, and if we assume the crystallinity of P3BT is 50% and PS is a part of the dielectric layer, $10^{19}/cm^3$ roughly corresponds to a gate bias of –10 V in this work. It implies that the threshold voltage of a vertical device should be –10 V more negative than that of a parallel device, which is consistent with Figures 5 and 6. At low $|V_g|$, the charge accumulation in crystalline P3BT facilitates the intra-domain charge transport, while the inter-domain hopping is limited inevitably by the trap in amorphous P3BT chains and lower HOMO levels. More negative gate bias fills these traps and at the same time lifts up the energy level of localized states in crystalline P3BT, which reduces the energetic barrier for charge hoping between amorphous and crystalline domains and thus induces a larger mobility. The relationship

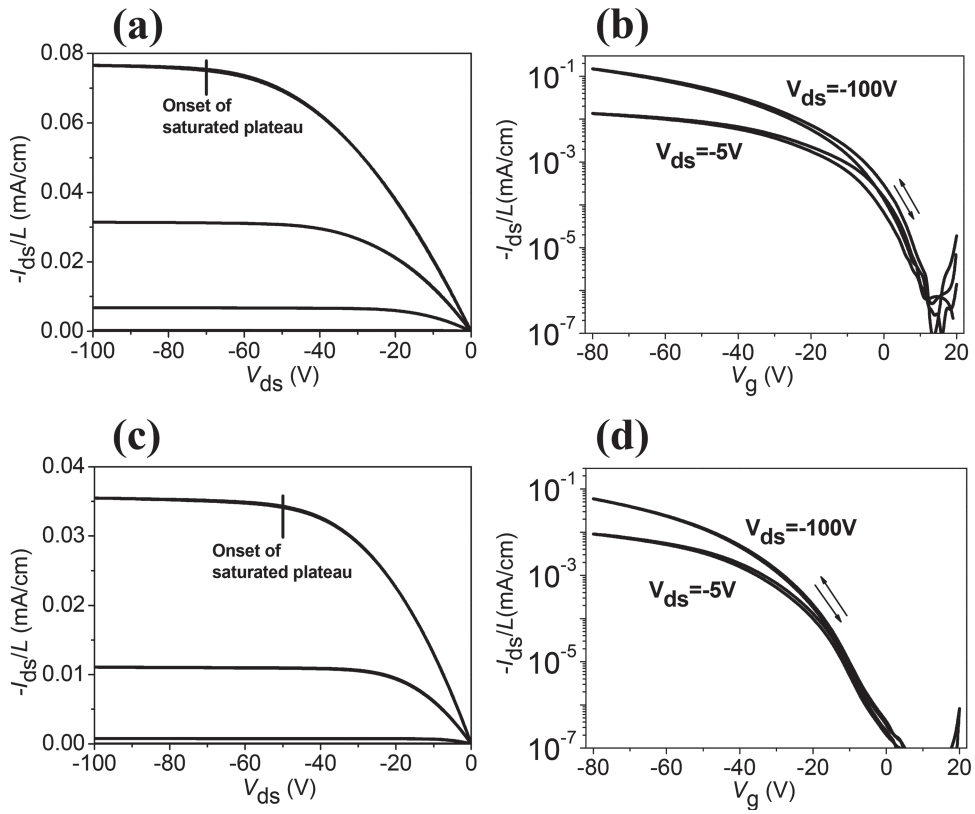

Figure 5. Field-effect transistor characteristics of aligned P3BT/PS (4 wt% P3BT) film. a,b) Source–drain current parallel to the direct-writing direction. c,d) Source–drain current vertical to direct-writing direction. a,c) Output characteristics, V_g = 0, −20, −40, −60 V. b,d) Transfer characteristics.

between charge accumulation and the energetic scheme is shown in Figure 6d, where −5.0 eV and −5.3 eV are the HOMO levels of crystalline and amorphous P3BT chain, respectively.

It is well known that the saturated feature in the output characteristics of FET is due to the narrow "pinch-off" region near the drain electrode, which bears most of the voltage drop across the channel as a result of low conductivity. From the output curves (Figure 5a,c), the onset of the saturated plateau of parallel transport is higher than that of vertical transport. For instance, in the case of V_g = −60 V, the former is about 20 V more negative than the latter. This means that, for vertical transport, the "pinch-off' region is easier to achieve. From the onset of the saturated plateau (for the case of V_g = −60 V) and V_{gd} =V_{gs}+V_{sd}, we get V_{gd} ≈ 10 V for parallel transport and V_{gd} ≈ −10 V for vertical transport. Because the "pinch-off' region is located at the drain side, it is concluded that for parallel transport more positive V_{gd} is necessary to "pinch off" the channel. This observation is consistent with the scheme shown in Figure 6d, where intra-domain hopping dominates parallel transport.

At low hole concentrations, inter-domain hopping is largely limited, while intra-domain charge transport leads to effective charge transport along the alignment direction. This is reminiscent of transistors based on aligned carbon nanotubes,[53] conjugated polymers,[63] or organic single crystals.[64–66] However, the mobility calculated from transistor characteristic is only a matter of I_{ds} on V_g. Pingel et al. reported the local mobility of P3HT as significantly different from the field-effect mobility.[57] Similarly, in this work, the apparent low μ_v at low hole concentrations is ascribed to the limited inter-domain charge transport. Once the carrier concentration is high enough to lift up the hole energy level in crystalline P3BT and more holes fill the traps in amorphous P3BT chains between nanowires, the field-effect mobility starts to rise more rapidly with V_g than in the parallel direction.

Figure 7a is the dependence of the field-effect mobility of aligned P3BT/PS blends on P3BT content. Our study shows that the aligned P3BT/PS blends have a high field-effect-transistor performance, in both the parallel and vertical directions. It means that, under gate-bias, inter-domain charge transport between P3BT nanowires is effective in P3BT/PS blends with a PS content of up to 96 wt%. Moreover, we observed a significant negative-shift of the threshold voltage of the blends as compared to neat P3BT, in both the parallel and vertical directions (Figure 7b). The Arrhenius equation $\mu = \mu_0 \exp(-E_a/kT)$ is used to calculate the activation energy, E_a, which is found to decrease with increasing of PS content. We ascribe this to the shielding of traps on the dielectric surface by the inert PS component, and/or the dilution of oxygen by the PS matrix. However, the activation energies along the parallel and vertical directions are comparable for P3BT/PS blends, which is consistent with the scheme shown in Figure 6d.

In P3BT/PS composites, the inter-domain space could be occupied not only by less crystalline P3BT chains, but also by the insulating PS matrix. In the latter case, charge hopping is supposed to be terminated. From this point of view, the effective P3BT concentration parallel to the alignment direction is

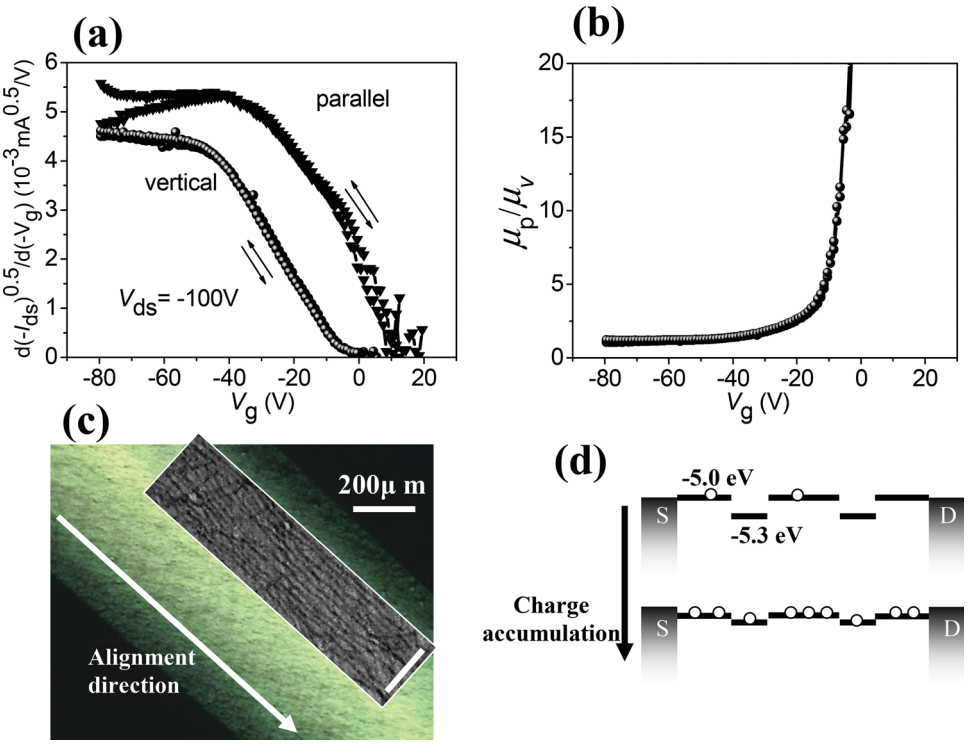

Figure 6. a) Dependence of $d(-I_{ds})^{0.5}/d(-V_g)$ on V_g for aligned P3BT/PS (4% P3BT). b) Dependence of μ_p/μ_v on gate bias V_g. c) CPOM of P3BT/PS blend stripe prepared by direct writing, and the angle between polarizer and direct-write direction is 45°. Inset is a TEM of P3BT/PS (4% P3BT) (scale bar, 200 nm). d) Energetic scheme for gate-bias-induced charge accumulation.

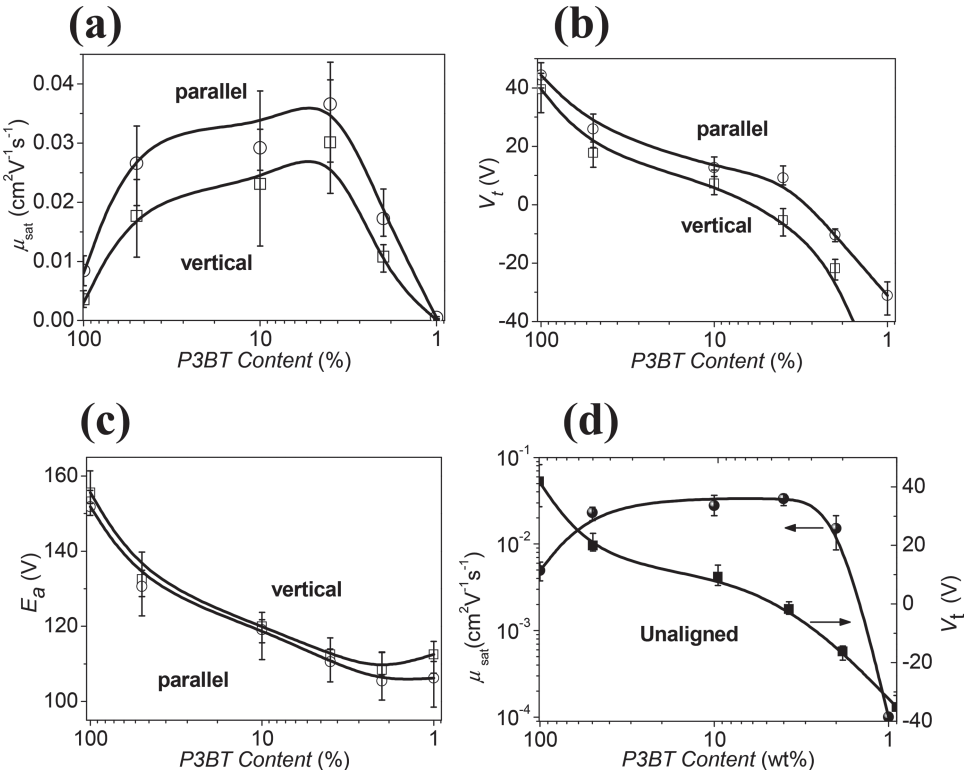

Figure 7. a–c) Dependence of anisotropic field-effect mobility (a), threshold voltage (b), and activation energy (c) of aligned P3BT/PS blends on P3BT content. d) Dependence of field-effect mobility and threshold voltage of unaligned (spincoated) P3BT/PS blends on P3BT content. The line are guides to eye, and the mobilities in (a) and (d) are extracted from the saturated mobility.

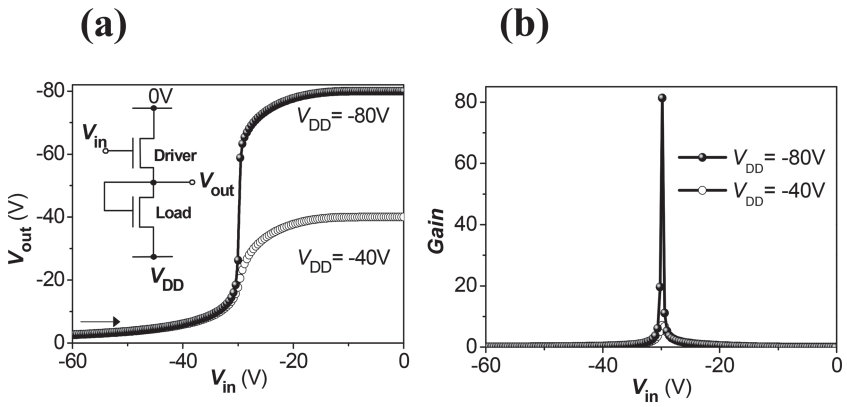

Figure 8. The application of anisotropic charge transport and tunable threshold voltages of aligned P3BT/PS blends. a) Transfer characteristics of a P3BT/PS digital inverter. Driver, P3BT/PS (3% P3BT) (vertical to film alignment); Load, P3BT/PS (10% P3BT) (parallel to film alignment). The driver works in enhancing mode, and the load works in depletion mode. b) Gain of the converter, as obtained from (a).

larger than that vertical to the alignment direction. Actually, by blending with insulating polymer, V_t of P3BT FET shifts towards the negative (Figure 7b). We ascribe this shift of V_t to the inter-domain charge transport, which gradually dominates the charge transport with increasing insulating content. In other words, in neat P3BT the carrier usually chooses the path with the least inter-domain bridges, while in the composite the carrier usually hops from one localized site to its nearest sites, as a result of percolation behavior. Therefore, inter-domain hopping plays a more important role in P3BT/PS composites, as compared to neat P3BT.

2.4. Application of Tunable Mobility and Threshold Voltage of Aligned Films

From the point view of application, tuning the V_t of P3BT/PS blends has great potential application in circuits[67,68] and memory.[69] For example, digital circuits usually need transistor units with different threshold voltages. In **Figure 8**, we demonstrate a digital inverter based on an anisotropic aligned P3BT/PS film, upon choosing the transistors with suitable mobility and V_t as load and driver. As shown in Figure 8a, the V_{out} features two plateaus. For a V_{in} between 0 V and −30 V, V_{out} denotes a digital 1, while for a V_{in} between −30 V and −60 V, V_{out} denotes a digital 0. Gain is defined as $|dV_{out}/dV_{in}|$, which represents the sensitivity of V_{out} to the change of V_{in} and thus is an important parameter for an inverter. The gain strongly depends on the mobility and threshold voltage of each transistor unit. As shown in Figure 8b, an inverter gain up to 80 can be realized using aligned P3BT/PS blend films, of which both the mobility and threshold voltage are tunable.

3. Conclusion

We have developed a direct-writing method to prepare aligned P3BT films, which show both high throughput and fidelity. The angle distribution of these P3BT nanowires, in both capillary and film, was quantitatively studied. Using this direct-writing method we obtained nematic alignment of both neat P3BT films and P3BT/PS blends. Subsequently, we investigated the field-effect transistor properties of aligned P3BT nanowires within a PS matrix. The increased mobility of P3BT/PS blends, as compared with neat P3BT, is observed in both the vertical and parallel directions. The anisotropic charge transport provides direct information on inter- and intra-domain charge transport, which helps us understand the high performance of transistors based on semiconductor/insulator polymer blends. Using this method, we comprehensively tuned the FET mobility and threshold voltage of semiconductor/insulator polymer blends, from which we realized a digital inverter with a gain of up to 80.

4. Experimental Section

Regioregular poly(3-butylthiophene) (P3BT) (97% head-to-tail regioregular conformation, Mw = 39.4 kDa, *PDI* = 2.29, Rieke Metals, Inc.). Amorphous (atactic) polystyrene (PS) (Mw = 124 kDa, *PDI* = 1.64, DaQing Petro Chemical Company) was further purified upon being dissolved in chloroform and precipitated by ethanol.

P3BT was dissolved in solvent ODCB by stirring, and elevated temperature 70–80 °C during stirring was used to achieve a solution with concentration 10 mg/mL. After being cooled to room temperature, the polymer solution was placed in dark and vibrationless environment to allow P3BT molecules to crystallize/self-assemble in solution. Glass capillary (diameter 80 μm) array was used for direct-writing process (writing speed 20 cm/s, film thickness 40–60 nm). The substrates (including glass for optical microscopy and silicon/SiO_2 for the FET) were cleaned by ultrasonic treatment in demineralized water, acetone, and isopropanol, in sequence.

Optical microscopy (OM) and polarized optical microscopy (POM) investigations were carried out by a Carl Zeiss A1m microscope equipped with Infinity 4–11 digital camera (Lumenera Co.).

Bright field transmission electron microscopy (TEM) was performed on a JEM-1011 (JEOL) operated at 100 kV. Thin films were firstly floated on deionized water, and then transferred onto copper grid. The samples were dried at room temperature for 24 h before TEM experiments.

For birefringence numerical simulations, as the prepared P3BT film is composed of numerous oriented P3BT nanowire domains, it is reasonable to assume that the deviation of these domains from direct-writing direction obeys normal distribution. So the distribution function of deviation of the nanowire can be described as $(1/\sigma)exp[-\alpha_i^2/(2\sigma^2)]$, where α_i is the deviation angle of the crystalline domain from the direct-writing direction, and σ is standard deviation. For convenience, here 100 000 random numbers α_i (i = 1-n) were generated in-between −90° and 90° by computer, and their occurrence probability is proportional to $(1/\sigma)exp[-\alpha_i^2/(2\sigma^2)]$. Least Squared Criterion is used to work out the most appropriate deviation σ, angle distribution and 2D orientation parameter f according to the experimental results.

P3BT and PS were dissolved in ODCB individually. After the crystallization of P3BT in solution, it was mixed with PS solution for direct writing/spincoating on n-doped silicon covered with 300 nm thick SiO_2 layer.

Bottom-gate, top-contact structures were finally completed by evaporation of 80–100 nm gold source/drain electrodes. Field-effect mobilities from saturation region were calculated according to $I_{ds} = (WC_i/2L)\mu_{sat}(V_g - V_t)^2$, where μ is the field-effect charge mobility

in saturation region; I_{ds} is source-drain current; C_i (12 nF cm^{-2}) is the capacitance per unit area; W (variable due to the size of polymer stripe) and L (100 μm) are the width and length of transistor channel, respectively, and; V_g and V_t are gate voltage and extrapolated threshold voltage, respectively.

Supporting Information

Supporting Information is available from the Wiley Online Library or from the author.

Acknowledgements

This work was supported by the National Natural Science Foundation of China (20990233), Hi-Tech Research and Development Program (863) of China (2011AA050524), Solar Energy Initiative (KGCX2-YW- 399 + 9) of the Chinese Academy of Sciences, and Alexander von Humboldt Fellowship. X. Y. would also like to thank the Fund for Distinguished Young Scholars (20925415) of NSFC. G. H. L thanks Dr. Haowei Tang, Dr. Laju Bu and Mr. Jun Li for experimental assistance. G. L thanks Prof. Dieter Neher, Dr. Patrick Pingel and Prof. James Watkins for inspirational discussion and support.

Received: March 2, 2014
Published online: May 22, 2014

[1] E. Menard, M. A. Meitl, Y. Sun, J.-U. Park, D. J.-L. Shir, Y.-S. Nam, S. Jeon, J. A. Rogers, *Chem. Rev.* **2007**, *107*, 1117.
[2] H. Li, B. C.-K. Tee, G. Giri, J. W. Chung, S. Y. Lee, Z. Bao, *Adv. Mater.* **2012**, *24*, 2588.
[3] A. Tracz, J. K. Jeszka, M. D. Watson, W. Pisula, K. Müllen, T. Pakula, *J. Am. Chem. Soc.* **2003**, *125*, 1682.
[4] Z. Hu, G. Baralia, V. Bayot, J.-F. Gohy, A. M. Jonas, *Nano Lett.* **2005**, *5*, 1738.
[5] M. Brinkmann, J.-C. Wittmann, *Adv. Mater.* **2006**, *18*, 860.
[6] M. Brinkmann, F. Chandezon, R. B. Pansu, C. Julien-Rabant, *Adv. Funct. Mater.* **2009**, *19*, 2759.
[7] C. Müller, M. Aghamohammadi, S. Himmelberger, P. Sonar, M. Garriga, A. Salleo, M. Campoy-Quiles, *Adv. Funct. Mater.* **2013**, *23*, 2368.
[8] D. Tu, S. Pagliara, A. Camposeo, G. Potente, E. Mele, R. Cingolani, D. Pisignano, *Adv. Funct. Mater.* **2011**, *21*, 1140.
[9] J. Liu, Y. Sun, L. Zheng, Y. Geng, Y. Han, *Polymer* **2013**, *54*, 423.
[10] H. N. Tsao, D. Cho, J. W. Andreasen, A. Rouhanipour, D. W. Breiby, W. Pisula, K. Müllen, *Adv. Mater.* **2009**, *21*, 209.
[11] W. Pisula, A. Menon, M. Stepputat, I. Lieberwirth, U. Kolb, A. Tracz, H. Sirringhaus, T. Pakula, K. Müllen, *Adv. Mater.* **2005**, *17*, 684.
[12] L. Hartmann, K. Tremel, S. Uttiya, E. Crossland, S. Ludwigs, N. Kayunkid, C. Vergnat, M. Brinkmann, *Adv. Funct. Mater.* **2011**, *21*, 4047.
[13] B. T. O'Connor, O. G. Reid, X. Zhang, R. J. Kline, L. J. Richter, D. J. Gundlach, D. M. DeLongchamp, M. F. Toney, N. Kopidakis, G. Rumbles, *Adv. Funct. Mater.* **2014**, DOI: 10.1002/adfm.201303351.
[14] G. Lu, L. Li, S. Li, Y. Qu, H. Tang, X. Yang, *Langmuir* **2009**, *25*, 3763.
[15] D. M. DeLongchamp, R. J. Kline, Y. Jung, D. S. Germack, E. K. Lin, A. J. Moad, L. J. Richter, M. F. Toney, M. Heeney, I. McCulloch, *ACS Nano* **2009**, *3*, 780.
[16] E. J. W. Crossland, K. Tremel, F. Fischer, K. Rahimi, G. Reiter, U. Steiner, S. Ludwigs, *Adv. Mater.* **2012**, *24*, 839.
[17] J. Liu, Y. Sun, X. Gao, R. Xing, L. Zheng, S. Wu, Y. Geng, Y. Han, *Langmuir* **2011**, *27*, 4212.
[18] M. Grell, D. D. C. Bradley, *Adv. Mater.* **1999**, *11*, 895.
[19] F. D. Stasio, P. Korniychuk, S. Brovelli, P. Uznanski, S. O. McDonnell, G. Winroth, H. L. Anderson, A. Tracz, F. Cacialli, *Adv. Mater.* **2011**, *23*, 1855.
[20] J. E. Smay, G. M. Gratson, R. F. Shepherd, J. Cesarano III, J. A. Lewis, *Adv. Mater.* **2002**, *14*, 1279.
[21] R. A. Barry III, R. F. Shepherd, J. N. Hanson, R. G. Nuzzo, P. Wiltzius, J. A. Lewis, *Adv. Mater.* **2009**, *21*, 2407.
[22] K. J. Ihn, J. Moulton, P. Smith, *J. Polym. Sci. Part B: Polym. Phys.* **1993**, *31*, 735.
[23] S. A. Chen, J. M. Ni, *Macromolecules* **1992**, *25*, 6081.
[24] T.-A. Chen, X. Wu, R. D. Rieke, *J. Am. Chem. Soc.* **1995**, *117*, 233.
[25] N. Stingelin-Stutzmann, E. Smits, H. Wondergem, C. Tanase, P. Blom, P. Smith, D. d. Leeuw, *Nat. Mater.* **2005**, *4*, 601
[26] C. P. Radano, O. A. Scherman, N. Stingelin-Stutzmann, C. Müller, D. W. Breiby, P. Smith, R. A. J. Janssen, E. W. Meijer, *J. Am. Chem. Soc.* **2005**, *127*, 12502.
[27] S. Goffri, C. Müller, N. Stingelin-Stutzmann, D. W. Breiby, C. P. Radano, J. W. Andreasen, R. Thompson, R. A. J. Janssen, M. M. Nielsen, P. Smith, H. Sirringhaus, *Nat. Mater.* **2006**, *5*, 950.
[28] P. Wolfer, C. Müller, P. Smith, M. A. Baklar, N. Stingelin-Stutzmann, *Synth. Met.* **2007**, *157*, 827.
[29] C. Müller, S. Goffri, D. W. Breiby, J. W. Andreasen, H. D. Chanzy, R. A. J. Janssen, M. M. Nielsen, C. P. Radano, H. Sirringhaus, P. Smith, N. Stingelin-Stutzmann, *Adv. Funct. Mater.* **2007**, *17*, 2674.
[30] A. Kumar, M. A. Baklar, K. Scott, T. Kreouzis, N. Stingelin-Stutzmann, *Adv. Mater.* **2009**, *21*, 4447.
[31] R. Hamilton, J. Smith, S. Ogier, M. Heeney, J. E. Anthony, I. McCulloch, J. Veres, D. D. C. Bradley, T. D. Anthopoulos, *Adv. Mater.* **2009**, *21*, 1166.
[32] J. Smith, R. Hamilton, Y. Qi, A. Kahn, D. D. C. Bradley, M. Heeney, I. McCulloch, T. D. Anthopoulos, *Adv. Funct. Mater.* **2010**, *20*, 2330.
[33] J. Sun, B.-J. Jung, T. Lee, L. Berger, J. Huang, Y. Liu, D. H. Reich, H. E. Katz, *ACS Appl. Mater. Interfaces* **2009**, *1*, 412.
[34] J. Liu, D. Haynes, C. Balliet, R. Zhang, T. Kowalewski, R. D. McCullough, *Adv. Funct. Mater.* **2012**, *22*, 1024.
[35] F. S. Kim, S. A. Jenekhe, *Macromolecules* **2012**, *45*, 7514.
[36] Y. Lin, Q. Wei, G. Qian, L. Yao, J. J. Watkins, *Macromolecules* **2012**, *45*, 8665.
[37] G. Lu, J. Blakesley, S. Himmelberger, P. Pingel, J. Frisch, I. Lieberwirth, I. Salzmann, M. Oehzelt, R. Di Pietro, A. Salleo, N. Koch, D. Neher, *Nat. Commun.* **2013**, *4*, 1588.
[38] G. Sauvé, R. D. McCullough, *Adv. Mater.* **2007**, *19*, 1822.
[39] L. Qiu, J. A. Lim, X. Wang, W. H. Lee, M. Hwang, K. Cho, *Adv. Mater.* **2008**, *20*, 1141.
[40] A. C. Arias, F. Endicott, R. A. Street, *Adv. Mater.* **2006**, *18*, 2900.
[41] Y. S. Chung, N. Shin, J. Kang, Y. Jo, V. M. Prabhu, S. K. Satija, R. J. Kline, D. M. DeLongchamp, M. F. Toney, M. A. Loth, B. Purushothaman, J. E. Anthony, D. Y. Yoon, *J. Am. Chem. Soc.* **2011**, *133*, 412.
[42] G. H. Lu, H. W. Tang, Y. P. Qu, L. G. Li, X. N. Yang, *Macromolecules* **2007**, *40*, 6579.
[43] G. Lu, H. Tang, Y. Huan, S. Li, L. Li, Y. Wang, X. Yang, *Adv. Funct. Mater.* **2010**, *20*, 1714.
[44] K. Vakhshouri, D. R. Kozub, C. Wang, A. Salleo, E. D. Gomez, *Phys. Rev. Lett.* **2012**, *108*, 026601.
[45] G. H. Lu, L. G. Li, X. N. Yang, *Adv. Mater.* **2007**, *19*, 3594.
[46] B. D. Wall, S. R. Diegelmann, S. Zhang, T. J. Dawidczyk, W. L. Wilson, H. E. Katz, H.-Q. Mao, J. D. Tovar, *Adv. Mater.* **2011**, *23*, 5009.

[47] R. S. Stein, *J. Polym. Sci.* **1958**, *31*, 327.
[48] R. S. Stein, *J. Polym. Sci.* **1958**, *31*, 335.
[49] W. Xu, L. Li, H. Tang, H. Li, X. Zhao, X. Yang, *J. Phys. Chem. B* **2011**, *115*, 6412.
[50] R. Steyrleuthner, M. Schubert, I. Howard, B. Klaumünzer, K. Schilling, Z. Chen, P. Saalfrank, F. Laquai, A. Facchetti, D. Neher, *J. Am. Chem. Soc.* **2012**, *134*, 18303.
[51] L. Xue, X. Gao, K. Zhao, J. Liu, X. Yu, Y. Han, *Nanotechnology* **2010**, *21*, 145303.
[52] X. Duan, C. Niu, V. Sahi, J. Chen, J. W. Parce, S. Empedocles, J. L. Goldman, *Nature* **2003**, *425*, 274.
[53] M. C. LeMieux, M. Roberts, S. Barman, Y. W. Jin, J. M. Kim, Z. Bao, *Science* **2008**, *321*, 101.
[54] L. Onsager, *Ann. N. Y. Acad. Sci.* **1949**, *51*, 627.
[55] J. P. F. Lagerwall, G. Scalia, *J. Mater. Chem.* **2008**, *18*, 2890.
[56] G. Lu, L. Bu, S. Li, X. Yang, *Adv. Mater.* **2014**, *26*, 2359.
[57] P. Pingel, A. Zen, R. D. Abellón, F. C. Grozema, L. D. A. Siebbeles, D. Neher, *Adv. Funct. Mater.* **2010**, *20*, 2286.
[58] A. Zen, J. Pflaum, S. Hirschmann, W. Zhuang, F. Jaiser, U. Asawapirom, J. P. Rabe, U. Scherf, D. Neher, *Adv. Funct. Mater.* **2004**, *14*, 757.
[59] S. Himmelberger, J. Dacuña, J. Rivnay, L. H. Jimison, T. McCarthy-Ward, M. Heeney, I. McCulloch, M. F. Toney, A. Salleo, *Adv. Funct. Mater.* **2012**, *23*, 2091.
[60] W. C. Tsoi, S. J. Spencer, L. Yang, A. M. Ballantyne, P. G. Nicholson, A. Turnbull, A. G. Shard, C. E. Murphy, D. D. C. Bradley, J. Nelson, J.-S. Kim, *Macromolecules* **2011**, *44*, 2944.
[61] D. P. McMahon, D. L. Cheung, A. Troisi, *J. Phys. Chem. Lett.* **2011**, *2*, 2737.
[62] H. Sirringhaus, *Adv. Mater.* **2005**, *17*, 2411.
[63] M. Zhang, H. N. Tsao, W. Pisula, C. Yang, A. K. Mishra, K. Müllen, *J. Am. Chem. Soc.* **2007**, *129*, 3472.
[64] J. H. Oh, H. W. Lee, S. Mannsfeld, R. M. Stoltenberg, E. Jung, Y. W. Jin, J. M. Kim, J.-B. Yood, Z. Bao, *Proc. Natl. Acad. Sci. USA* **2009**, *106*, 6065.
[65] C. Mitsui, J. Soeda, K. Miwa, H. Tsuji, J. Takeya, E. Nakamura, *J. Am. Chem. Soc.* **2012**, *134*, 5448.
[66] H. N. Tsao, K. Müllen, *Chem. Soc. Rev.* **2010**, *39*, 2372.
[67] C. Huang, J. E. West, H. E. Katz, *Adv. Funct. Mater.* **2007**, *17*, 142.
[68] G. Gelinck, P. Heremans, K. Nomoto, T. D. Anthopoulos, *Adv. Mater.* **2010**, *22*, 3778.
[69] Q. Wei, Y. Lin, E. R. Anderson, A. L. Briseno, S. P. Gido, J. J. Watkins, *ACS Nano* **2012**, *6*, 1188.